Supporting Information

Remodeling arteries: studying the mechanical properties of 3D-bioprinted hybrid photoresponsive materials

Uxue Aizarna Lopetegui,[a,b] Clara Garcia,[a,c] Carlos Renero-Lecuna,[a,c] Patricia Gonzalez,[a] Irune Villaluenga,[d,e] Miguel A. del Pozo,[f] Miguel Sánchez-Álvarez,[f,g] Malou Henriksen-Lacey,[a,c*] and Dorleta Jimenez de Aberasturi[a,c,e*]

[a]*CIC biomaGUNE, Basque Research and Technology Alliance (BRTA), Miramon Pasealekua, 194, 20014 Donostia-San Sebastián, Gipuzkoa, Spain*
[b]*Department of Applied Chemistry, University of the Basque Country, 20018 Donostia-San Sebastián, Gipuzkoa, Spain*
[c] *Centro de Investigación Biomédica en Red de Bioingeniería, Biomateriales y Nanomedicina (CIBER-BBN, ISCIII), 20014 Donostia-San Sebastián, Gipuzkoa, Spain*
[d]*POLYMAT, University of the Basque Country UPV/EHU, 20018 Donostia-San Sebastián, Gipuzkoa, Spain*
[e] Ikerbasque, Basque Foundation for Science, 48009 Bilbao, Spain
[f]*Mechanoadaptation and Caveolar Biology Laboratory. Novel Mechanisms of Atherosclerosis Program. Centro Nacional de Investigaciones Cardiovasculares (CNIC), 28029 Madrid, Spain*
[g] *Department of Metabolic and Immunity Diseases. Instituto de Investigaciones Biomédicas "Alberto Sols", 28029 Madrid, Spain*

Table of Contents

1. Rheological and thermo-characterization characterization of thermoresponsive inks

1.1. Temperature ramps of the different pNIPAm-PEGDA formulations

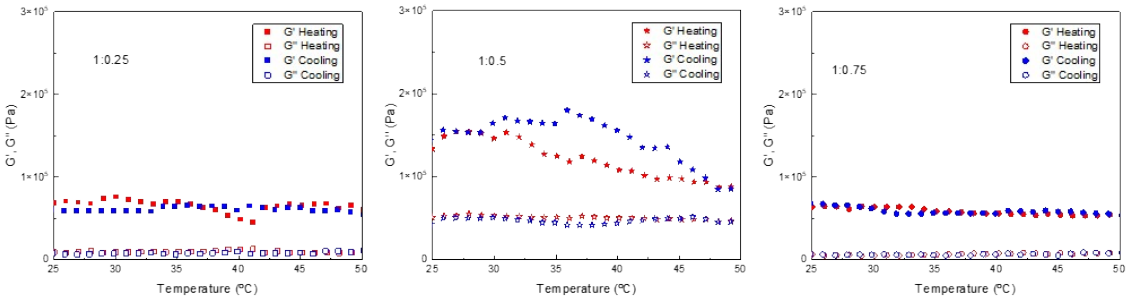

Figure S1. Temperature ramps with heating (from 25 to 50 °C at 1 °C/min) and cooling (from 50 to 25 °C at 1 °C/min) cycles for controls made using varying NIPAM-PEGDA ratios.

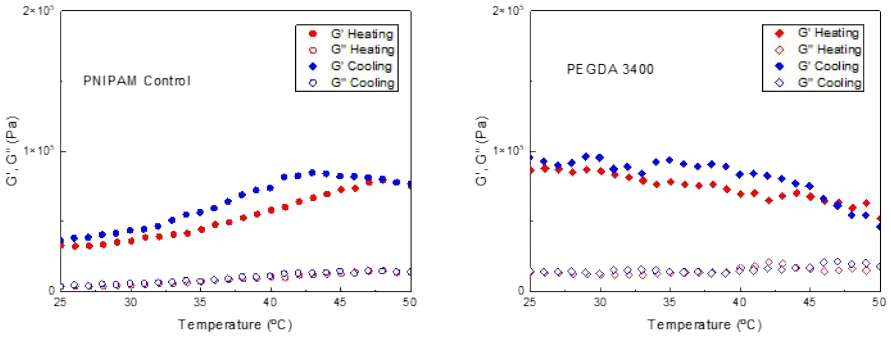

Figure S2. Temperature ramps with heating (from 25 to 50 °C at 1 °C/min) and cooling (from 50 to 25 °C at 1 °C/min) cycles for controls made using pNIPAM (left) and PEGDA 3400 (right).

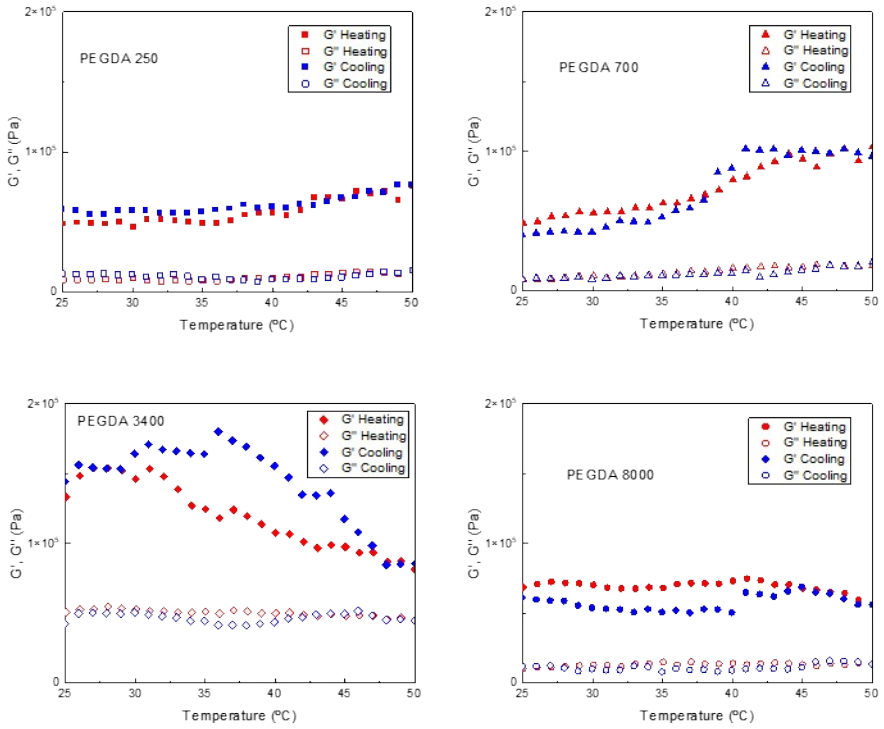

Figure S3. Temperature ramps with heating (from 25 to 50 °C at 1 °C/min) and cooling (from 50 to 25 °C at 1 °C/min) cycles for controls made using NIPAM-PEGDA hydrogels varying PEGDA molecular weight.

1.2. Differential Scanning Calorimetry of the thermoresponsive formulations

The lower critical solution temperature of the pNIPAm – PEGDA (3400 Da) gels at a 1:0.5 polymeric ratio with 0, 0.5 and 1 mM of AuNRs was measured by Differential Scanning Calorimetry (DSC). To obtain the LCST of each of the compositions, three heating and cooling sweeps from 20 to 60 °C were performed. The heating curves of the first sweeps (black) were discarded, ensuring that any possible artifact was removed, and the system was stabilized for the following measurements. The average inflection points of the heating curves of the second (blue) and third (purple) curves were calculated for obtaining the LCST for each gel (shown in Table S1). The cooling curves of the three sweeps (represented in red, green and brown, respectively) indicated the reversibility of the system but were not considered for calculating the transition temperature of the material.

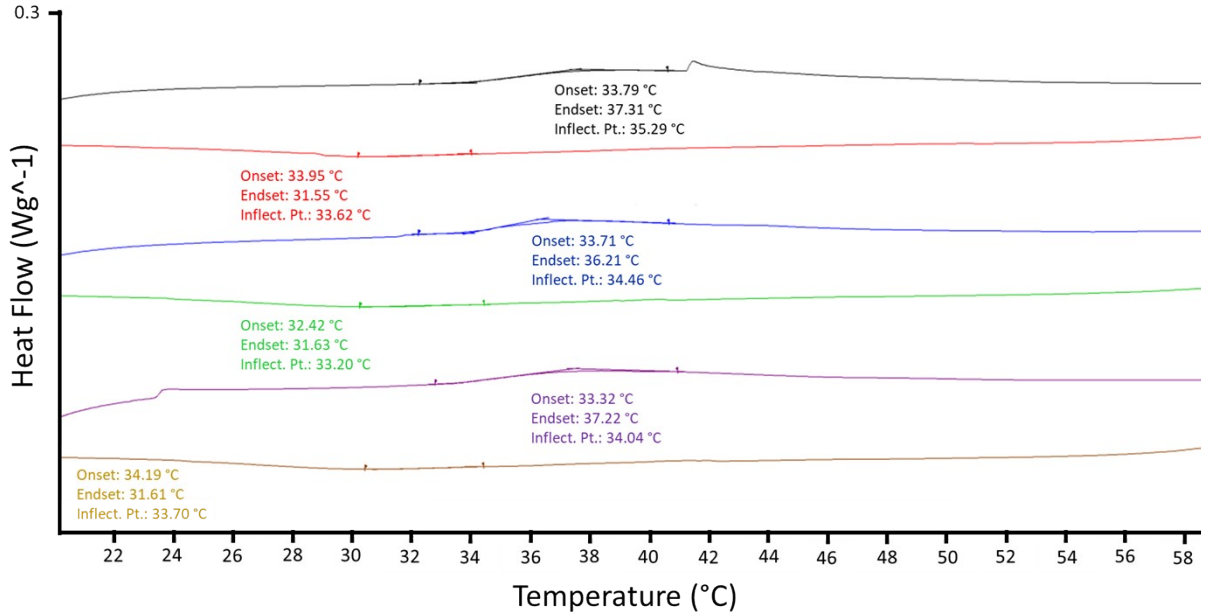

Figure S4. DSC curves of gel without AuNRs.

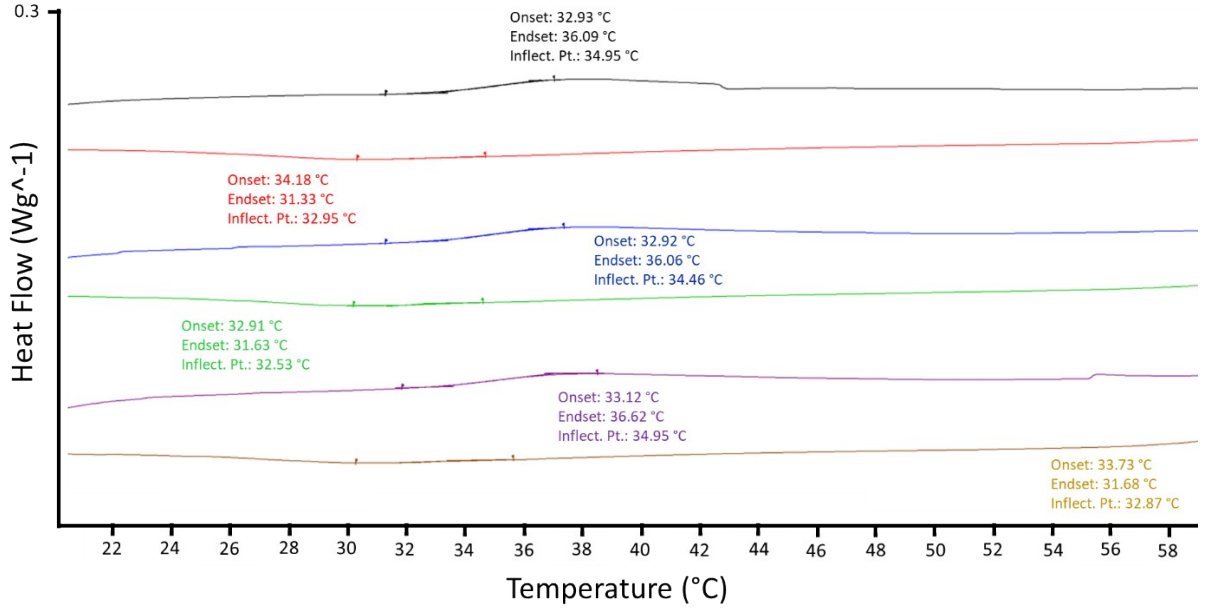

Figure S5. DSC curves of 0.5 mM of AuNRs containing gel.

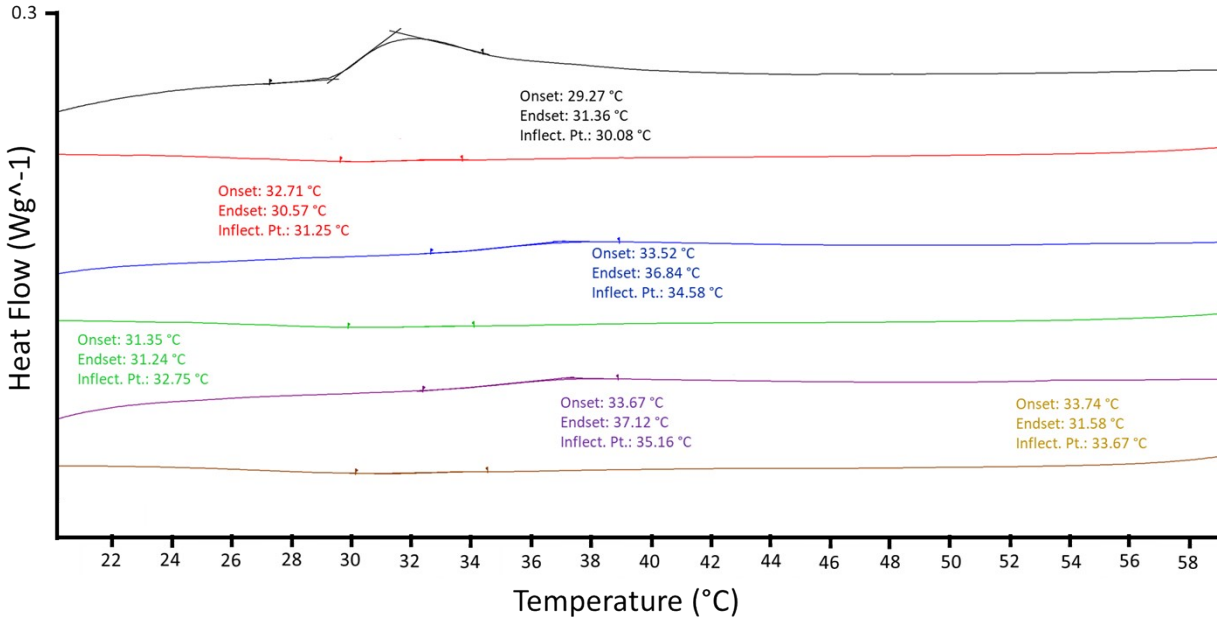

Figure S6. DSC curves of 1 mM of AuNRs containing gel.

Table S1. LCST values calculated from the DSC measurements, corresponding to the average of the second (blue) and third (purple) heating curves of the sweeps.

[AuNRs]	LCST
0 mM	34.25 ± 0.29 °C
0.5 mM	34.70 ± 0.34 °C
1 mM	34.87 ± 0.41 °C

1.3. SAXS measurements of the thermoresponsive formulations

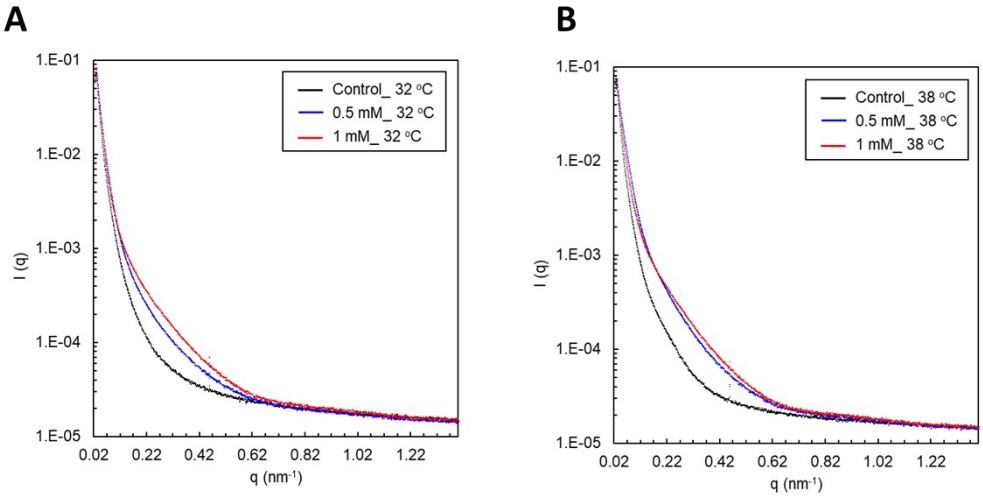

Figure S7. Characterization of the gel (pNIPAm-PEGDA (3400 Da; 1:0.5 ratio)) morphological changes for mixtures containing 0 mM [Au^0] 0.5 mM [Au^0] (blue) and 1 mM [Au^0] (red) at A) 32 °C and B) 38 °C above LCST.

1.4. Viscoelastic properties of the formulations

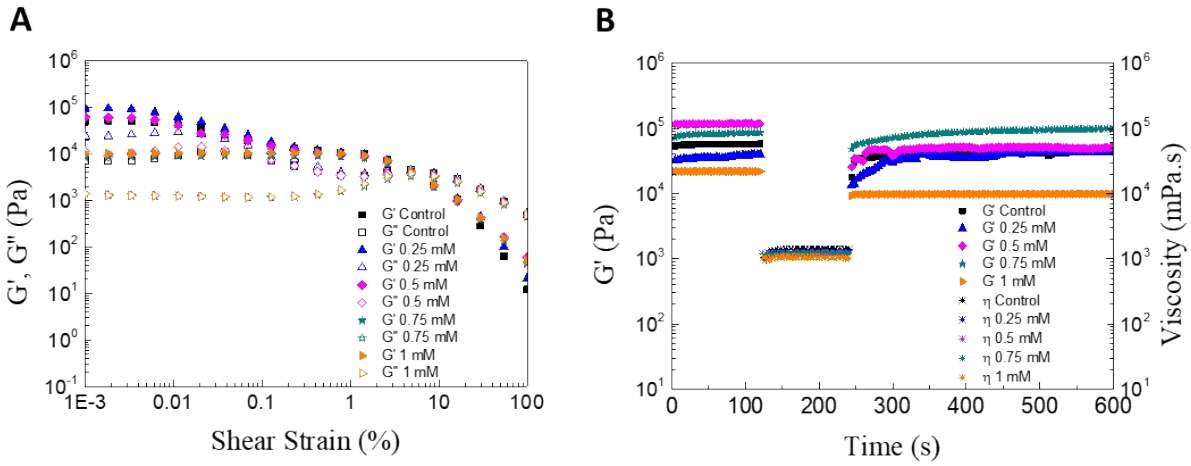

Figure S8. Rheological measurements for the characterization of the viscoelastic properties of the inks and hydrogels containing different AuNR concentrations. (A) Strain sweep for the different ink formulations, and B) thixotropy tests for the different hydrogel formulations.

1.5. Laser-based heating characterization of the thermoresponsive inks

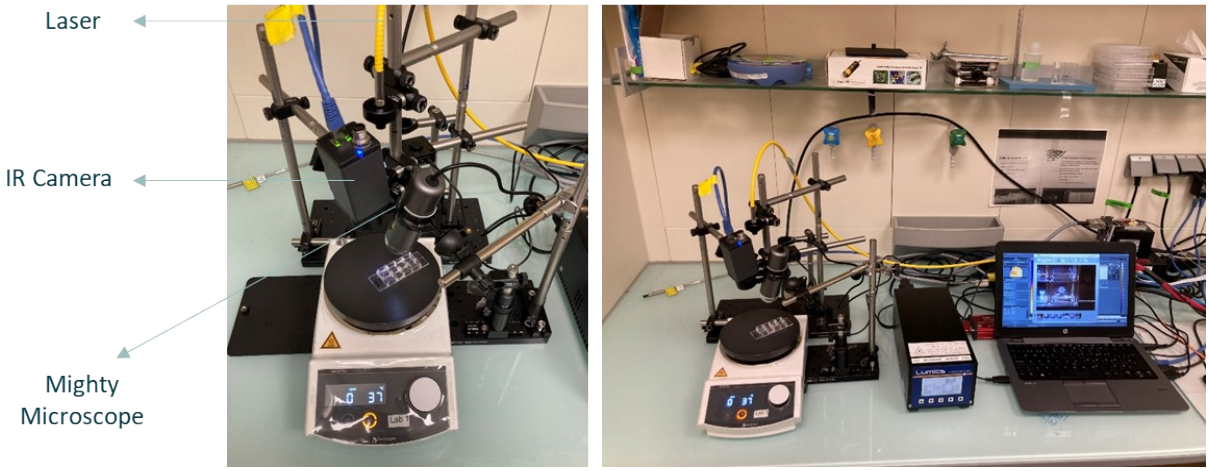

Figure S9. Setup of the heating unit consisting of the laser, infrared camara, a "Mighty" microscope and the heating plate. The laser is a high-power diode laser (Lumics, LuOcean Mini 8, LU0808D105) with 4 fixed wavelengths (785, 808, 980 and 1064 nm), measurements were performed with 808 nm matching with AuNRs plasmon band position. The system is coupled to a thermal camera (FLIR AX5), which allows measuring the temperature of the system while heating.

Table S2. Summary of the maximum temperature (T_{max}) and change in temperature for each thermoresponsive gel upon continuous irradiation. Various AuNR concentrations and laser powers were tested.

Continuous Illumination	Laser Density Power	T max (at plateau)	ΔT
0.25 mM	1 W/cm2	33.25 °C	6.5 °C
	1.5 W/cm2	36.04 °C	9.2 °C
	2 W/cm2	38.95 °C	11.9 °C
0.5 mM	1 W/cm2	37.86 °C	9.6 °C
	1.5 W/cm2	40.73 °C	12.6 °C
	2 W/cm2	44.56 °C	16.4 °C
0.75 mM	1 W/cm2	37.64 °C	11.9 °C
	1.5 W/cm2	42.22 °C	16.2 °C
	2 W/cm2	46.76 °C	20.2 °C
1 mM	1 W/cm2	41.57 °C	14.1 °C
	1.5 W/cm2	46.45 °C	19.0 °C
	2 W/cm2	51.48 °C	24.4 °C

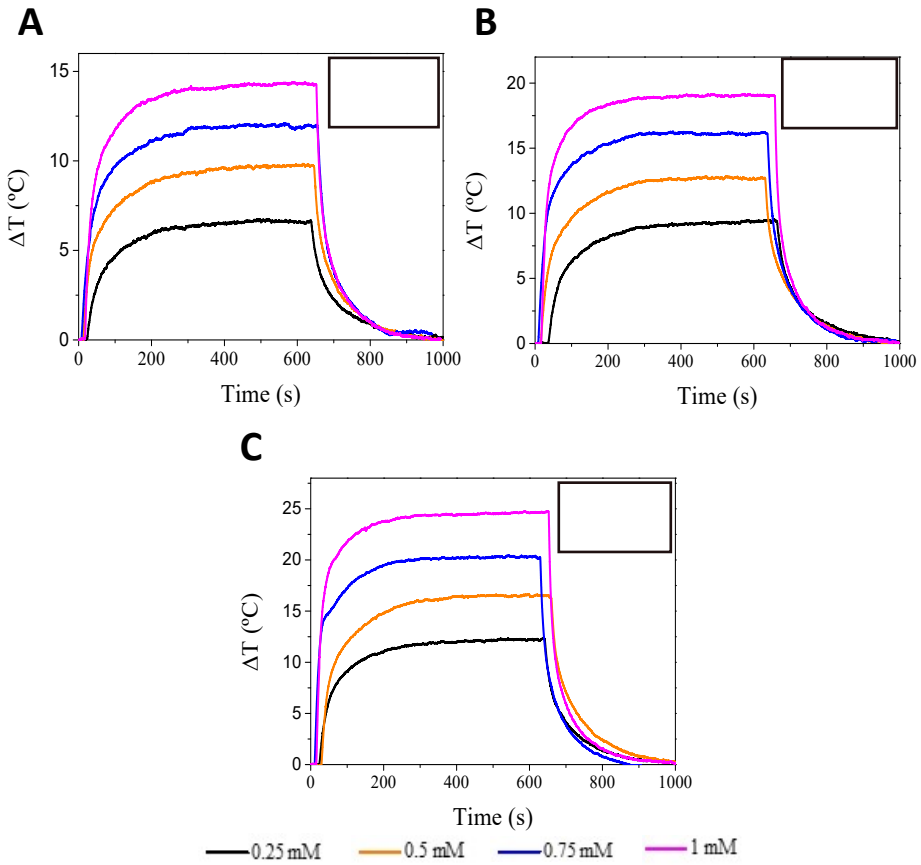

Figure S10. Temperature change profiles of thermoresponsive gels containing AuNRs (0.25 – 1 mM) when irradiated with a CW laser at a density power of (A) 1 W/cm^2, (B) 1.5 W/cm^2 and (C) 2 W/cm^2 under 808 nm laser excitation.

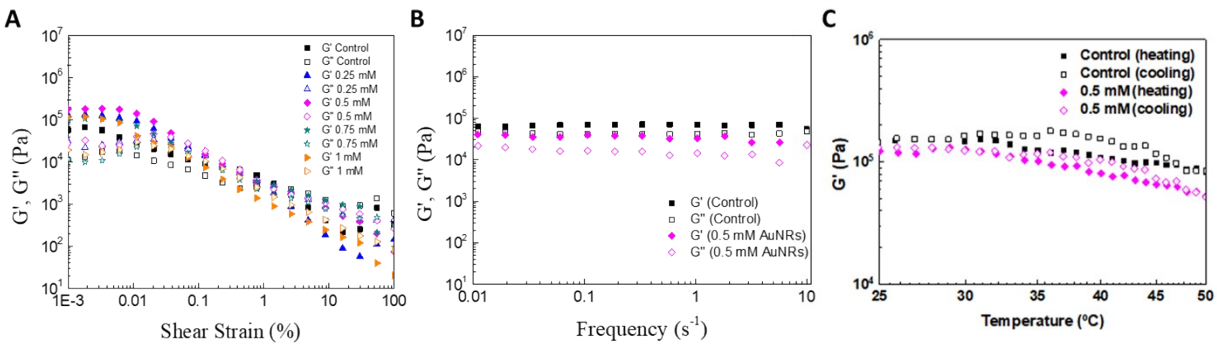

Figure S11. Rheological characterization of crosslinked hydrogel discs varying AuNP concentration. **(**A) Strain sweep, (B) frequency sweeps for the control and 0.5mM AuNRs containing gels, and (C) temperature ramps with heating (from 25 to 50 °C at 1 °C/min) and cooling (from 50 to 25 °C at 1 °C/min) cycles.

2. Structural characterization of the thermoresponsive inks

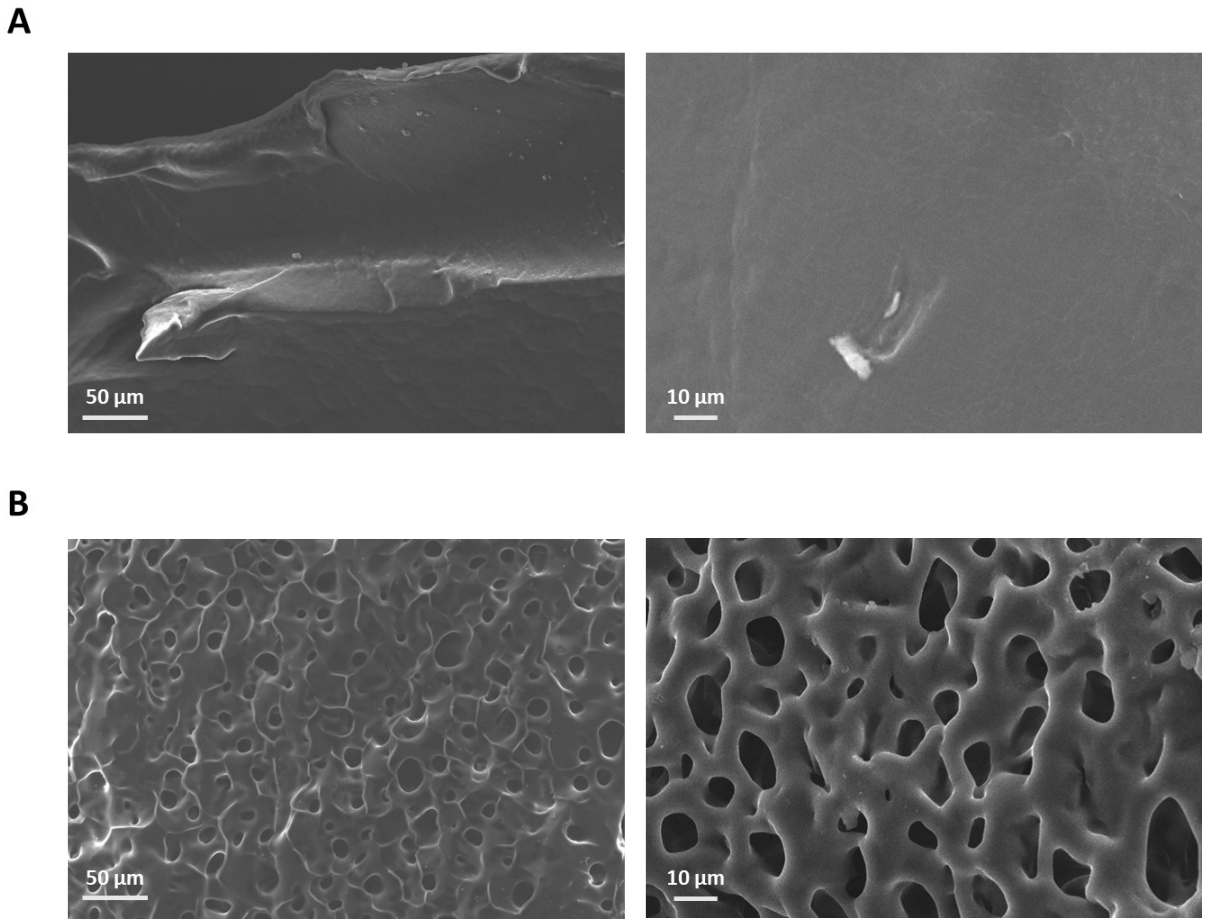

Figure S12. Scanning Electron Microscopy images of the thermoresponsive gels pre (A), zoom image (right) and (B) after removal of the sacrificial material, Pluronic F127.

3. Pulsed laser irradiation of the thermoresponsive inks

Table S3. Summary of the maximum temperature reached and temperature increase when illuminating the selected 0.5 mM gel in both continuous and pulsed mode (4 s on – 16 s off) at different laser powers.

Laser Density Power	T max (at plateau)	ΔT
1 W/cm^2	37.7 °C	10.2 °C
1.5 W/cm^2	41.8 °C	14.8 °C
2 W/cm^2	46.4 °C	19.2 °C
2.5 W/cm^2	50.4 °C	22.5 °C
3 W/cm^2	53.6 °C	25.6 °C

Table S4. Summary of the change in temperatures for each thermoresponsive gel upon pulsed laser irradiation. Various AuNR concentrations and laser powers were tested using a cycle of 4 s laser on followed by 16 s laser off.

Pulsed Illumination	Laser Density Power	ΔT
0. 25 mM	1 W/cm^2	0.9 °C
	1.5 W/cm^2	1.7 °C
	2 W/cm^2	2.5 °C
0.5 mM	1 W/cm^2	0.8 °C
	1.5 W/cm^2	1.6 °C
	2 W/cm^2	2.6 °C
0.75 mM	1 W/cm^2	0.7 °C
	1.5 W/cm^2	3 °C
	2 W/cm^2	4.5 °C
1 mM	1 W/cm^2	2.5 °C
	1.5 W/cm^2	4.4 °C
	2 W/cm^2	7.3 °C

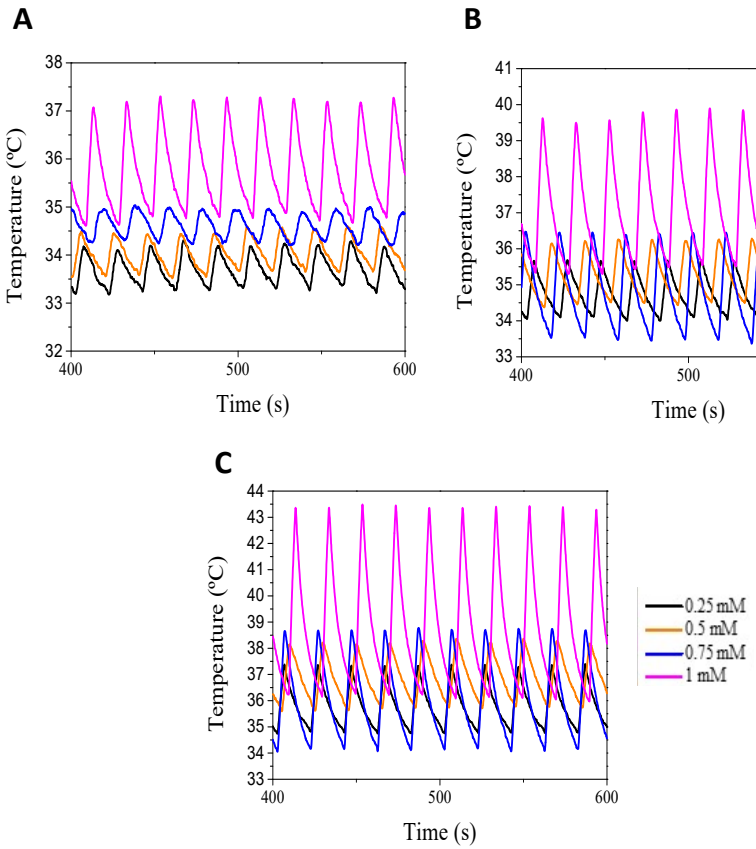

Figure S13. Temperature change profiles of different crosslinked gels when irradiated under pulsed mode at a density power of (A) 1 W/cm^2, (B) 1.5 W/cm^2 and (C) 2 W/cm^2 and at 808 nm excitation wavelength.

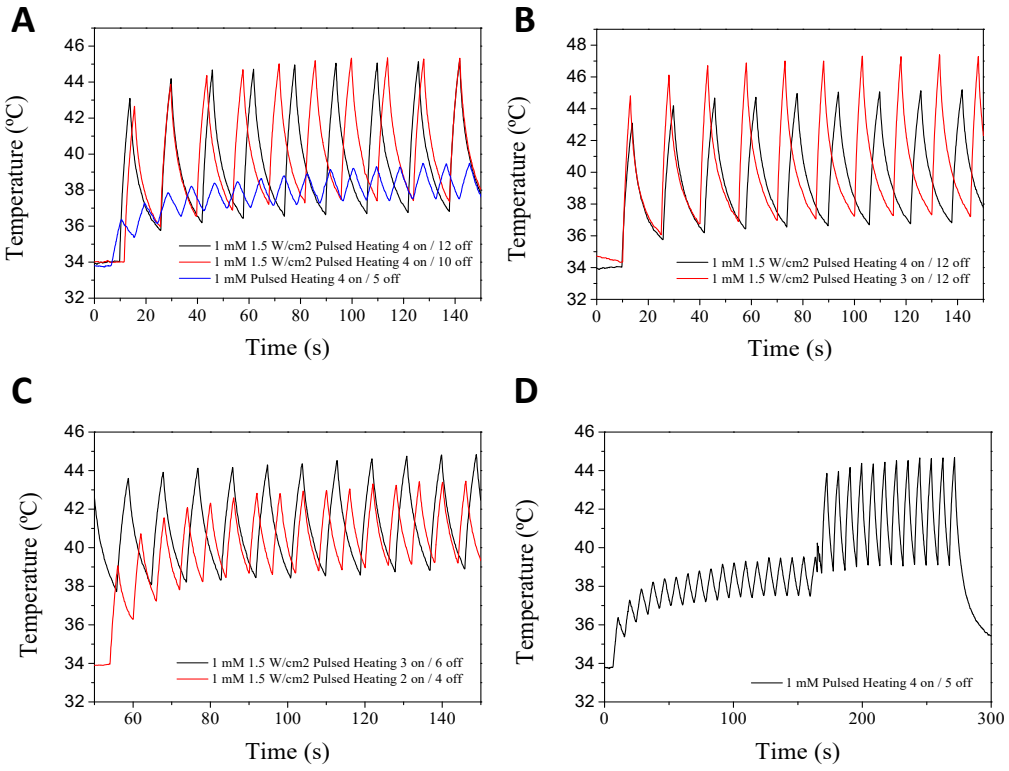

Figure S14. Temperature change profiles obtained during optimization of the laser pulse frequency and period under 808 nm wavelength excitation.

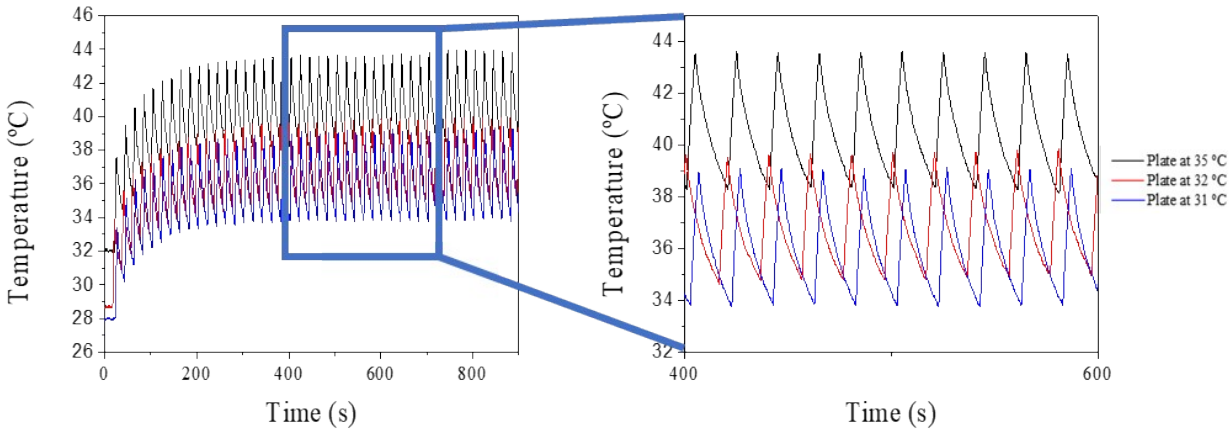

Figure S15. Pulsed heating (4 on – 16 off) curves when irradiating the sample at 2.5 W/cm^2 and using different heating plate temperatures.

The absorbance spectra of the crosslinked hydrogels were measured pre and post heating by UV−vis−NIR spectroscopy where the gels were directly inserted into the measuring cuvettes and immersed in distilled water. The noise in the absorbance spectra arises from the inhomogeneities found in the light path, as the gels could not be fixed within the cuvettes. However, no significant shift indicative of AuNR reshaping (AuNR reshaping is normally visualized by a blue shift of the plasmon band), is observed, verifying the non-invasiveness of expanding and contracting the gels with the laser.

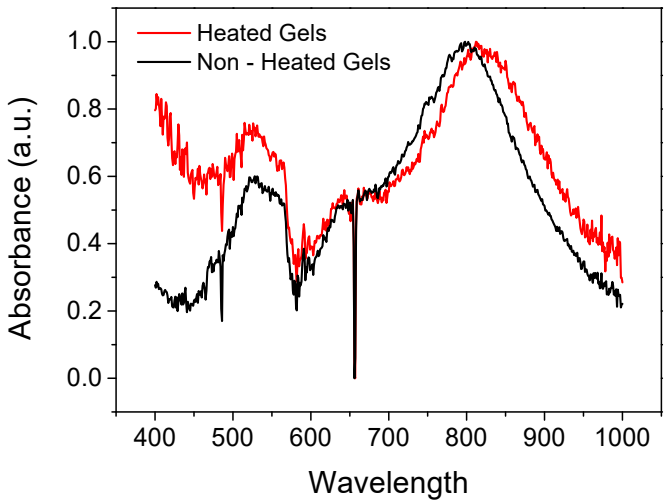

Figure S16. Absorbance spectra of irradiated and non-irradiated gels.

4. Image and video analysis of the expansion and contraction of the gels

Two approaches were considered to quantify the possible contraction of the 3D printed cylinders when irradiated with the laser. Firstly, the lumen area of the cylinder was segmented and the difference in the total area (number of pixels within the segmented region multiplied by pixel's area) was assessed overtime (**Figure S17 A** and **B**). From this data (**Figure S17B**) it was concluded that the difference in radius of the segmented area was approximately of 0.9 mm (from $A = \pi r^2$). However, considering that the expansion and contraction of the material occurs in all directions, and not just inwards towards the lumen, we also evaluated the cylindrical structure (**Figure S17 C** and **D**). The change in the mean radius

of the segmentation of the cylinder was ca. 1.5 mm. The difference in the radius calculated by both segmentation approaches is in the same order of magnitude and showed that the expansion and contraction of the material occurs in all directions (the difference in the lumen radius being close to half of the difference of the cylinder itself).

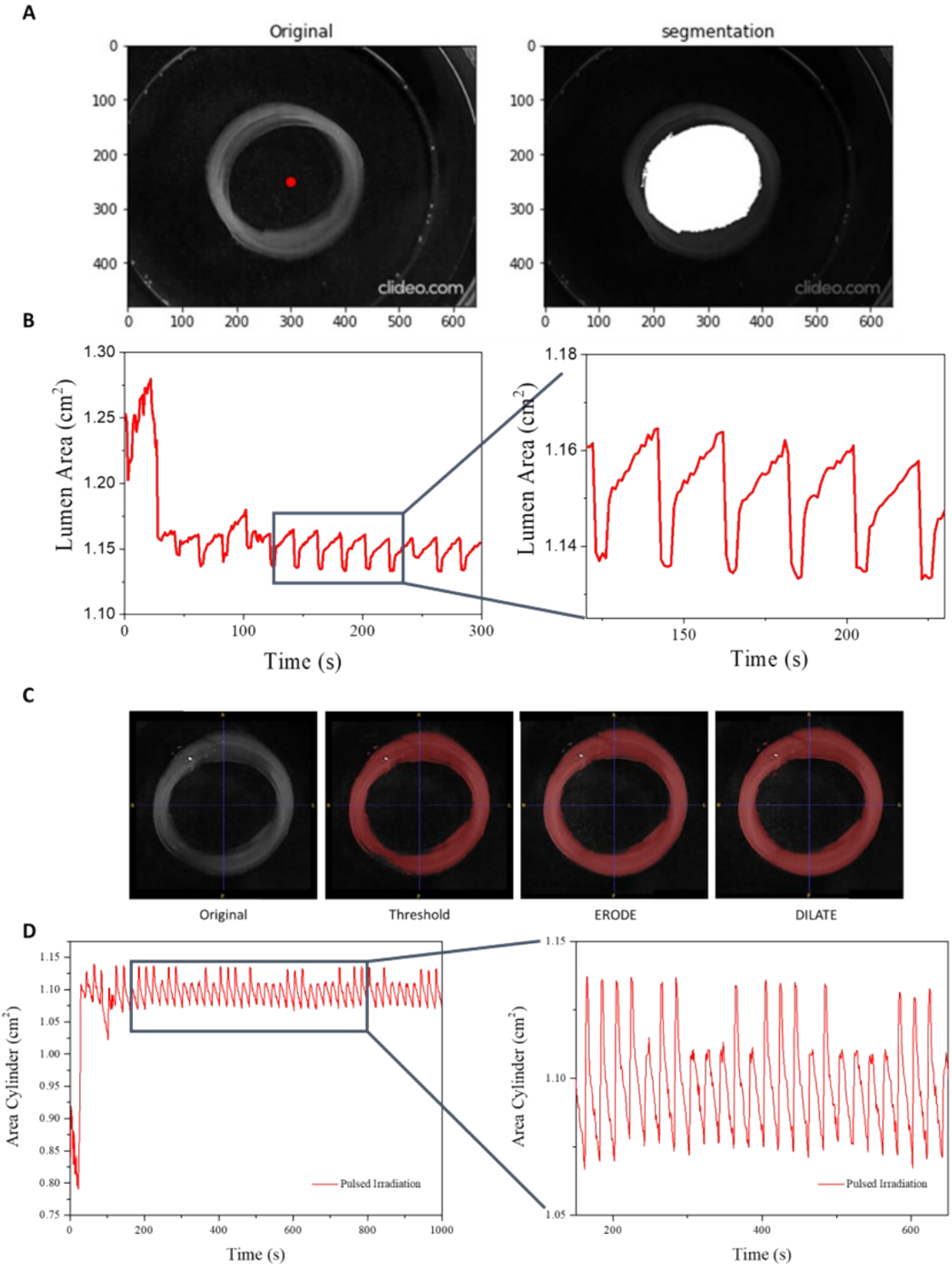

Figure S17. Different segmentations of the cylinder for the contraction and expansion analysis. (A) Segmentation of the lumen, (B) changes of lumen area over time, (C) visualization of the different steps of the cylinder area segmentation process in ITK-SNAP, and (D) corresponding area changes over time.

5. 3D printing of multi-layered systems

5.1 Cell Viability

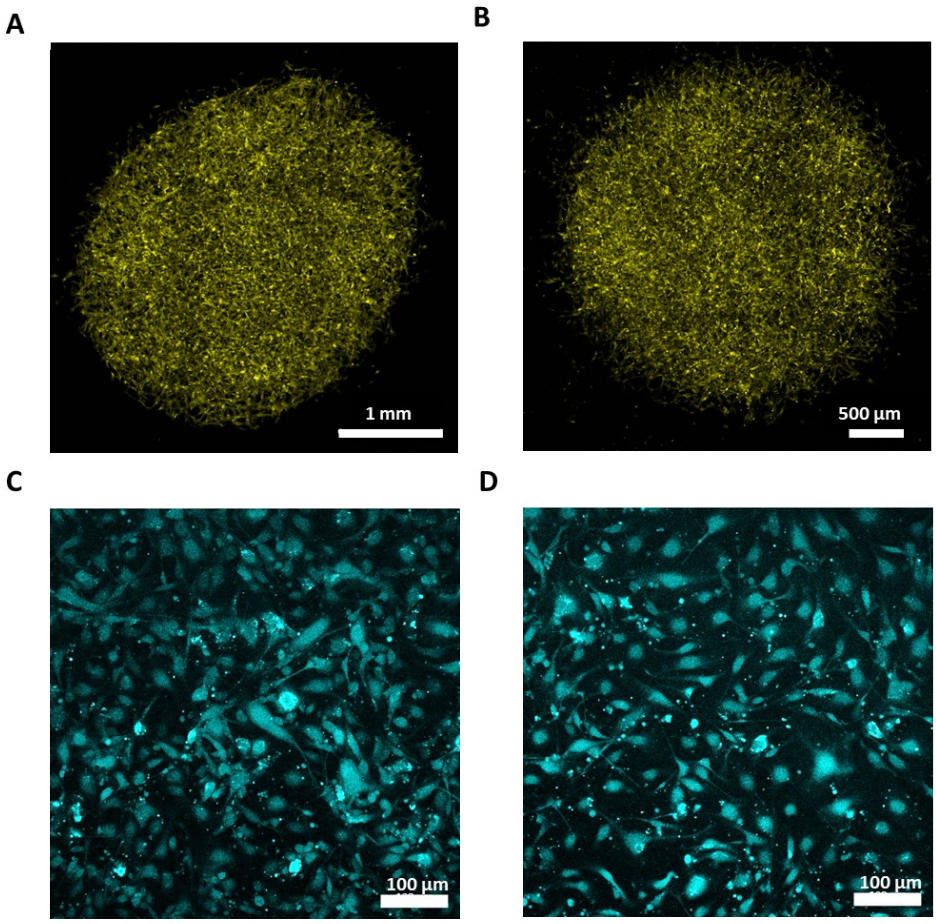

Figure S18. SMCs labelled with Cell Tracker deep red (A) pre and (B) post printing, and endothelial cells stained with Cell Tracker blue (C) pre and (D) post printing.

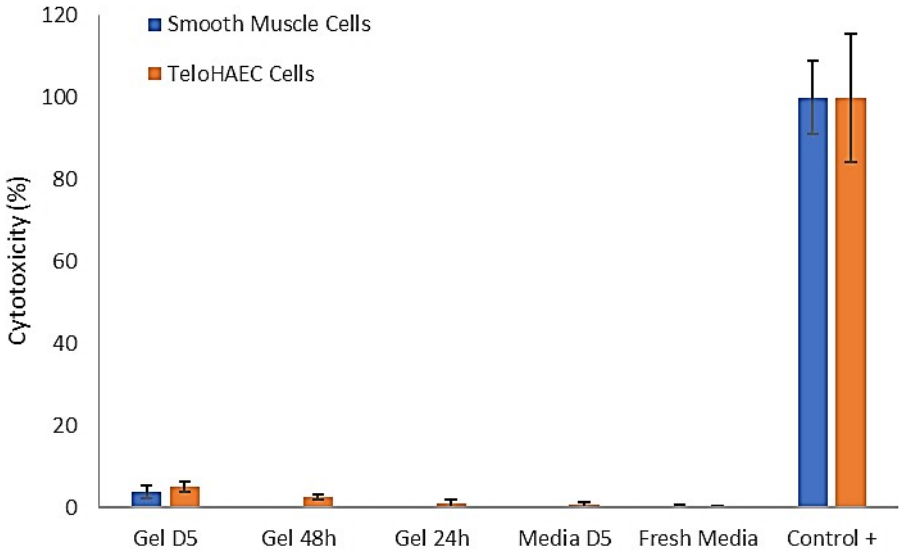

Figure S19. Analysis of cell viability of SMCs and endothelial TeloHAEC cell lines using the LDH kit. Cells were exposed to vascular cell media that had previously been incubated with thermoresponsive gels containing AuNRs (0.5 mM) for 5 days (D5), 48h and 24h. Controls included maximum LDH release (10 % v/v lysis buffer resulting in total cell death), and spontaneous LDH release (non-treated cells) with 5 day-old media and fresh media.

Table S5. Concentration of gold detected in thermoresponsive gels after their incubation in vascular cell media for 5 days, 48 h and 24 h by ICP-MS.

	Mean [Au^0] (nM)	% of Au Released
Gel Day 5	4.51	0.90 %
Gel 48h	2.21	0.44 %
Gel 24h	2.16	0.43 %

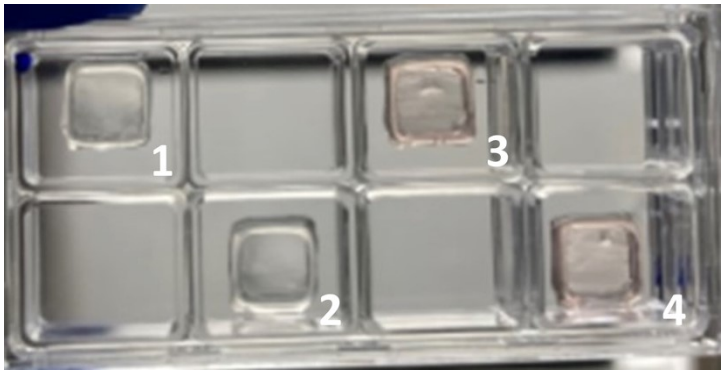

Figure S20. 3D printed thermoresponsive gels in 8 well Ibitreat plates. Gels with (well 1,2) and without (well 3,4) AuNRs are shown.

5.2 Structural characterization of the 3D-printed multi-layered model

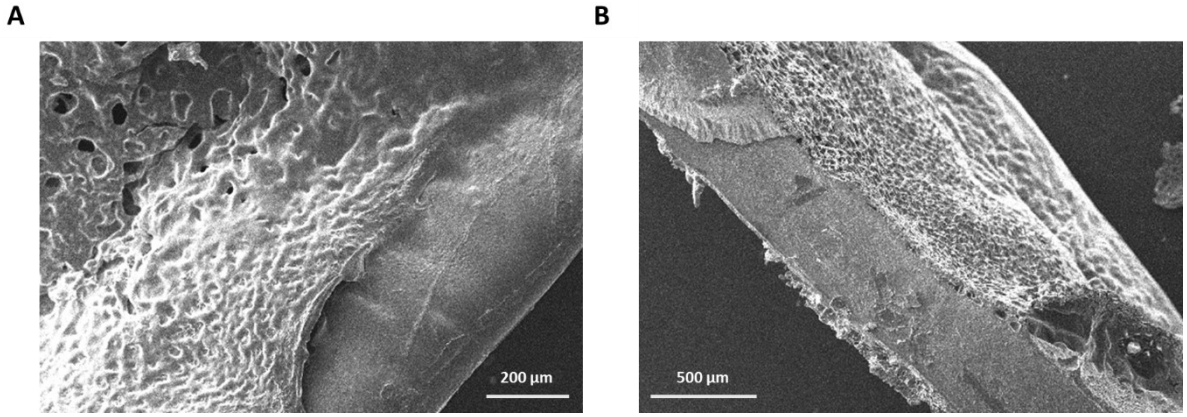

Figure S21. SEM images showing the interface between Matrigel and the thermoresponsive layer when liquid is removed from its surface, seen from the (A) top and (B) side.

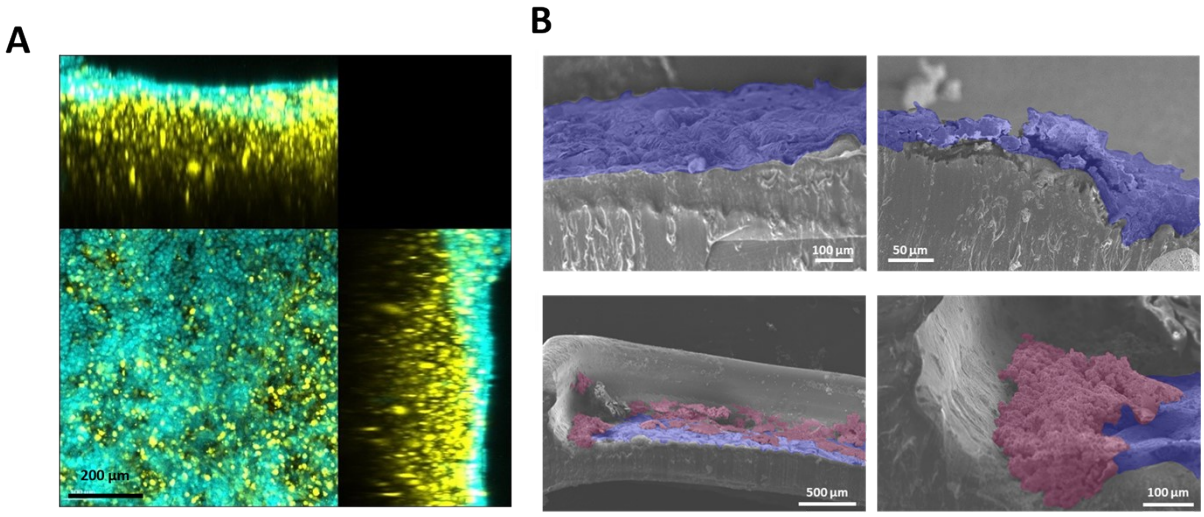

Figure S22. A) Live cell fluorescence orthogonal confocal image showing SMCs (yellow) embedded in the Matrigel and endothelial cells (blue). B) SEM images of the interface between the different materials showing SMCs (false coloured in blue) embedded in the Matrigel on top of the thermoresponsive gel and endothelial cells (false coloured in pink) collecting at the borders.

5.3. 3D printing parameters of the different materials of the model

Table S6. Printing parameters of the thermoresponsive formulation

Printing Parameters (Microextrusion - Plunger dispenser)	
Metallic Tip	0.25 mm (long)
Feed Rate	5 mm/s
Cartridge Heater	35 ºC
Square dimensions	l = 6 mm 1 filled layer 5 empty layers
Line spacing	0.25 mm
Crosslinking	40” after filled layer + 40” at end

Table S7. Cell Friendly printing parameters of SMCs embedded in Matrigel and endothelial in cell media.

Printing Parameters (Inkjet printing)		
	SMCs in Matrigel	**Endothelial in cell media**
Jetting	0.1 mm microvalve	0.1 mm microvalve
Pressure	0.05 MPa	0.05 MPa
Feed Rate	15 mm/s	15 mm/s

Layer Thickness	0.1 mm	0.1 mm
Square dimensions	l = 6 mm 5 horizontal and 5 vertical lines are printed forming a square (x3 layers)	l = 6 mm 5 horizontal and 5 vertical lines are printed forming a square (x3 layers)

5.4 Functional characterization of the 3D printed model

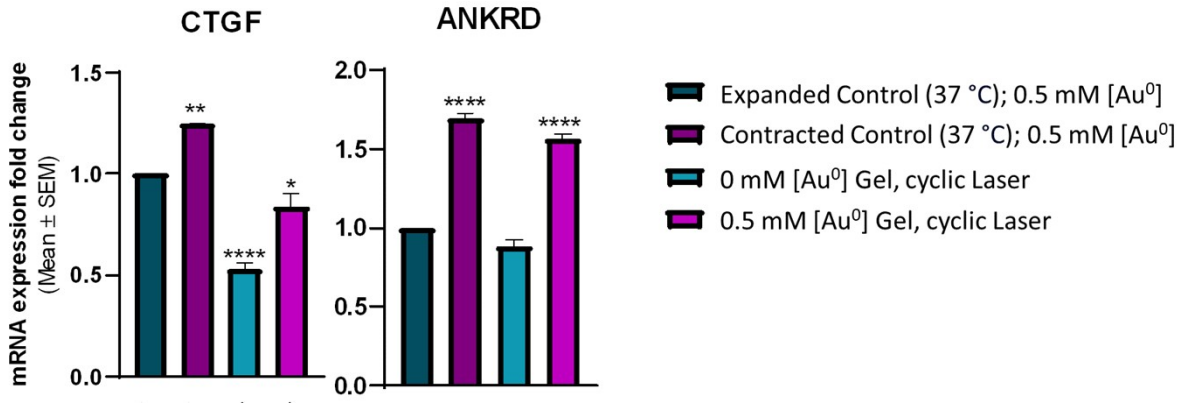

Figure S23. qRT-PCR analysis of ANKRD1 and CTGF genes associated with the YAP/TAZ pathway. Cells were recovered from models exposed to different conditions including AuNR (0.5 mM [Au^0]) containing gels incubated at 33 °C (green) and 37 °C (purple), and the gels (both control gel (no AuNRs: 0 mM [Au^0] (blue)) and AuNR (0.5 mM [Au^0] (fuchsia)) containing gel) exposed to cyclic laser irradiation (2.5 w/cm^2, 4s on/ 16 s off) for 4h. Data shows Mean +/- SEM with significance differences (One-way ANOVA followed by Dunnett´s Multiple Comparisons test) tested against Expanded Control (*P ≤ 0.05, **P ≤ 0.01, ***P ≤ 0.001, ****P ≤ 0.0001).

Table S8. PCR primers.

Primer Name	Oligonucleotide Sequence
SNAIL FW	GAGGCGGTGGCAGACTAG
SNAIL RV	GACACATCGGTCAGACCAG
SLUG FW	TGCGATGCCCAGTCTAGAAA
SLUG RV	GTGTCCTTGAAGCAACCAGG
GAPDH FW	CAGAACATCATCCCTGCATCCACT
GAPDH RW	GTTGCTGTTGAAGTCACAGGAGAC
TGF-B FW	GCCGCTGCCCATCGTGTACTA
TGF-B RV	GGCTTGGGCACGGGTGTCC
CTGF FW	ACCGACTGGAAGACACGTTTG
CTGF RV	CCAGGTCAGCTTCGCAAGG
ANKRD1 FW	AGTAGAGGAACTGGTCACTGG
ANKRD1 RV	TGTTTCTCGCTTTTCCACTGTT